Science and Technology Indonesia
e-ISSN:2580-4391 *p*-ISSN:2580-4405
Vol. 10, No. 2, April 2025

Research Paper

Preparation and Characterization of ZnO-Fe_2O_3 Nanocomposite Using Green Synthesis Method and Its Application in Powder Pyrotechnics

Evie Lestariana[1,2*], Heru Supriyatno[1], Hamonangan Rekso Diputro Sitompul[1], Afni Restasari[3], Yoki Yulizar[2]

[1]*Research Center for Rocket Technology, Research Organization of Aeronautics and Space, National Research and Innovation Agency, Bogor, 16350, Indonesia*
[2]*Department of Chemistry, Faculty of Mathematics and Natural Science, University of Indonesia, Depok, 16424, Indonesia*
[3]*Research Center for Biomass and Bioproducts, National Agency for Research and Innovation, Cibinong, 16911, Indonesia*
***Corresponding author**: evie.lestariana@ui.ac.id*

Abstract
Nanocomposites are often used as a catalyst in the pyrolysis of Al/Mg/KNO_3 rocket igniter charge. Because the synthesis of the nanocomposites has a negative impact on the environment, in this study, the nanocomposite of ZnO-Fe_2O_3 was synthesized using a green synthesis method based on the aqueous fraction of *Syzygium polyanthum* (Wight) Walp. leaf extract. The secondary metabolites contained in the extract were tested. ZnO-Fe_2O_3 nanocomposite was characterized using Ultra-Violet-Visible Diffuse Reflectance Spectroscopy (UV Vis-DRS), Fourier Transform Infra-Red Spectroscopy (FT-IR), X-ray Diffraction (XRD), Particle Size Analyzer (PSA), Scanning Electron Microscope-Energy Dispersive X-Ray Spectroscopy (SEM-EDS), and Transmission Electron Microscope (TEM). The thermal decomposition process of Al/Mg/KNO_3 with and without ZnO-Fe_2O_3 nanocomposite was analyzed using Differential Thermal Analysis (DTA) and Thermogravimetry Analysis (TGA). As a result, ZnO-Fe_2O_3 nanocomposite is successfully synthesized, proven by UV-Vis DRS, FT-IR, XRD, and SEM-EDS analysis. It highlights the effectiveness of aqueous leaves extract of Syzygium polyanthum (Wight) Walp. as a capping agent because of the secondary metabolites. Based on PSA and TEM characterization, the particle size is 17.37 nm. The TGA curves demonstrate that the addition of ZnO-Fe_2O_3 nanocomposite lowers the activation energy for decomposition of Al/Mg/KNO_3, from 58.71 kJ/mol to 52.07 kJ/mol, as well as reduces the stage in the decomposition process. A particular reason lies on the role of ZnO-Fe_2O_3 nanocomposite in reducing the activation energy of the thermal decomposition of KNO_3.

Keywords
Green Synthesis, ZnO-Fe_2O_3 Nanocomposite, Al/Mg/KNO_3 Pyrotechnic Powder, Thermal Decomposition

Received: 18 July 2024, Accepted: 16 January 2025
https://doi.org/10.26554/sti.2025.10.2.493-503

1. INTRODUCTION

Pyrotechnics are a mixture of oxidizers, fuels, binders and additives which have ability to react rapidly (Ineichen and Berger, 2004). One of the usage is to ignite and burn rocket fuel (propellant) (Ineichen and Berger, 2004; León et al., 2024). The fuel and oxidizer of pyrotechnics can be metal, alloy, or compound (Ineichen and Berger, 2004). Element fuels include aluminum, magnesium, titanium, iron, manganese, tungsten, boron, etc, while compound fuels are hydrocarbons, picrates, carbohydrates, arsenic sulfide, antimony sulfide, etc (Ineichen and Berger, 2004). The oxidants can be metal oxides or peroxides, nitrates, chlorates, and chromates of alkali and alkaline earth metals (Aegerter et al., 2023; Dave et al., 2016; Lackner et al., 2013), while the binder is a polymer (Ineichen and Berger, 2004). Due to the function of accelerating the decomposition process, the crucial additive in pyrotechnics is a catalyst (Ineichen and Berger, 2004).

For catalyst in pyrotechnics, because of the various oxidation states and the unique electronic configurations, transition metal oxide nanoparticles (TMON) such as iron oxide (Fe_2O_3), manganese oxide (MnO_3 or Mn_2O_3), and chromium (III) oxide (Cr_2O_3) are highly effective (Ravanbod and Pouretedal, 2016). Furthermore, nanocatalysts are preferred to micro-sized and bulky catalysts because the activity increases with a larger surface area (Ravanbod and Pouretedal, 2016). Thus, combining two types of TMONs, ZnO-Fe_2O_3 nanocomposites is potential to be used in pyrotechnics (Ravanbod and Pouretedal, 2016; Yaou Balarabe et al., 2023). However, the conventional synthesis of ZnO-Fe_2O_3 nanocomposite causes a negative impact on the human health and environment because of the toxicity of the chemicals used in the process (Kharissova et al., 2019). In this case, green synthesis is important (Ying et al., 2022;Kharissova et al., 2019). In addition to reducing the

toxic, green synthesis is reported to reduce energy consumption and increase production (Osman et al., 2024). Similar to natural oil-based green plasticizer developed for rocket propellant (Restasari et al., 2024), ZnO-Fe_2O_3 nanocomposite is potential to be synthesized by using plant-based extract which has a function as a capping or reducing agent which is a molecule that stabilizes nanoparticles and prevent them from aggregating or coagulating to form larger particles (Javed et al., 2020; Kharissova et al., 2019; Ying et al., 2022).

Several studies have been conducted in green synthesis of ZnO and Fe_2O_3 nanoparticles (Al-Darwesh et al., 2024; Kiwumulo et al., 2022). Various extracts of stem, stem bark, leaf, flower, fruit, fruit peel, seed, and marine plants have been used for synthesis of ZnO and Fe_2O_3 nanoparticles (Abdelbaky et al., 2023; Abdelmigid et al., 2022; Al-Darwesh et al., 2024; Buarki et al., 2022; Faisal et al., 2021; Islam et al., 2024; Kiwumulo et al., 2022; Lakshmnarayanan et al., 2021; Naiel et al., 2022; Thi et al., 2020). In addition, for ZnO nanoparticle, extract of callus, aerial and onion (*Allium cepa*) have also been used (Al-Darwesh et al., 2024; Islam et al., 2024), while for Fe_2O_3 nanoparticle, soya bean sprout, stolon, biowastes, gum, green coffee, cloves, bacteria, and fungi have been involved in the synthesis (Kiwumulo et al., 2022; Mohamed et al., 2023; Zunigaga-Miranda et al., 2023). However, different from ZnO and Fe_2O_3 nanoparticles, investigation about green synthesis of nanocomposite is still limited.

Green synthesis of ZnO-FeO nanocomposite is reported by using aqueous extract of leaves of *Eucaliptus globulus* Labill, *Cuphea aequipetala* Cav., and *Blepharis maderaspantensis* (Abbas et al., 2020; Reyes-Perez et al., 2023). Leaves extract of *Phoenix dactylifera* L. is reported to be involved in green synthesis of Zn-Fe_2O_4 nanocomposite (Abdullah et al., 2024). For synthesis of ZnO-Fe_2O_3 nanocomposite, chitosan is used (Al-Rajhi et al., 2024). Exploration of the use of aqueous extract of leaves on the synthesis of ZnO-Fe_2O_3 nanocomposite is still rare.

Because the usage of aqueous extract of leaves has been proven to be successful in the synthesis of nanoparticles and nanocomposites, choosing a plant which has many leaves and grows easily will bring benefit. Among plants, with the ability to grow large and reach a height of 20-25 meters in lowlands in Indonesia, up to 1400 meters above sea level, *Syzygium polyanthum* (Wight) Walp is a potential source for the extract (Ali et al., 2022). Previous research report that it can be used in synthesis on silver, and ZnO nanoparticles (Khan et al., 2023; Lestariana et al., 2024). The success may lie on various secondary metabolites contained in the extract of *Syzygium polyanthum* (Wight) Walp such as alkaloids, saponins, steroids, phenols, and flavonoids which can support its function as a capping agent (Javed et al., 2020; Widjajakusuma et al., 2019). Thus, the novelty of this work is the use of aqueous leaves extract of *Syzygium polyanthum* (Wight) Walp in synthesizing ZnO-Fe_2O_3 nanocomposite to be applied in pyrotechnic powder.

To determine the effectivity of the novel catalyst of pyrotechnics, investigation of the decomposition process, by which complex compounds are decomposed or destroyed or broken down into simpler compounds, is essential (Goncalves et al., 2017; Zheng et al., 2022). The decomposition process caused by exposure to heat is called pyrolysis (thermal decomposition) (Zheng et al., 2022) . The pyrolysis can be observed using thermal analysis instruments such as DTA and TGA (Zheng et al., 2022). In DTA and TGA, the changes in mass and thermal profile of a material are continuously recorded while the sample is heated in an oven under specific conditions (Zheng et al., 2022). Based on the data of DTA-TGA, a mathematical model of the kinetic of the pyrotechnic decomposition process can be built to determine activation energy, Arrhenius constant and reaction rate constant (Goncalves et al., 2017). Those parameters serve as a guide for the product storage system of pyrotechnics and rocket ignition devices (Goncalves et al., 2017; Hatakeyama et al., 1998).

The importance of green synthesis and thermal decomposition analysis, this work has two aims. The first aim is to investigate the ability of *Syzygium polyanthum* (Wight) Walp. leaves extract as capping agent in synthesis of ZnO-Fe_2O_3 nanocomposite. Second aim is to determine the effect of the ZnO-Fe_2O_3 nanocomposite resulted from the green synthesis on the thermal decomposition process of Al/Mg/KNO_3 pyrotechnic powder. The incorporation of ZnO-Fe_2O_3 nanocomposite to pyrotechnic powder should alter their combustion performance compared to normal pyrotechnic powder counterparts.

2. EXPERIMENTAL SECTION

2.1 Materials

In this work, materials used to obtain leaf extract were leaf powder (*Syzygium polyanthum* (Wight) Walp.) obtained from Tropical Biopharmaceutical Study Center of LPPM IPB-Bogor, methanol, n-hexane, and distilled water. For the phytochemical tests, the materials included distilled water, HCl 37% solution, Wagner's reagent, NaOH, acetic anhydride, chloroform, H_2SO_4, $FeCl_3$, while for synthesis ZnO-Fe_2O_3 nanocomposite, $Zn(NO_3)_2.4H_2O$, $Fe(NO_3)_3.9H_2O$, potassium nitrate (KNO_3) 99.0% were used. In addition, producing pyrotechnic powder involves the addition of aluminum (Al) powder 90.9% and magnesium (Mg) powder 0.006-0.3 mm. All chemicals were pro-analysis grade and purchased from Merck and used without further purification.

2.2 Instruments

FT-IR (Shimadzu Prestige 21), 4000-400 cm^{-1}, was used to analyze the functional groups of aqueous fraction of the leaf extract of *Syzygium polyanthum* (Wight) Walp., the synthesized nanoparticles and ZnO-Fe_2O_3 nanocomposite. Identifying the maximum absorption of ZnO-Fe_2O_3 nanocomposites was conducted by using UV-Vis DRS instrument (Hitachi UH-5300), 200-800 nm. Crystal characteristics were obtained from XRD (Bruker, X-ray source: Cobalt (Co)) analysis with a diffraction angle of 10 - 120°. Particle characterizations of ZnO-Fe_2O_3 nanocomposite include distribution of particle size and charge using PSA (PSA Nanoplus) with dynamic light scattering system (DLS), and shape morphology using

SEM-EDS (Phenom) of 15 kV. TEM (Tecnai G2 20S-Twin Function) 200 kV, sub-Ångström resolution of 0.24 nm (dot) and 0.188 nm (line), magnification range of 25x-1030kx, CCD Camera and EDS (Energy Dispersive X-Ray Spectroscopy) allowed to analyze elemental composition (Sebehanie, 2017). The thermal decomposition of Al/Mg/KNO_3/ZnO/Fe_2O_3 pyrotechnic powder was measured using DTA and TGA with nitrogen gas, heating rate of 10°C/min, from 30°C to 1000°C (Sivapirakasam et al., 2010).

2.3 Methods

2.3.1 Sample Preparation and Phytochemical Testing of *Syzygium polyanthum* (Wight) Walp. Leaf Extract

Fresh leaves are washed, dried at room temperature and in the oven. Dried leaves are ground into a fine powder using a mechanical grinding tool. Fifty grams of *Syzygium polyanthum* (Wight) Walp. leaf powder was placed in an Erlenmeyer flask. Two hundred and fifty milliliters of methanol was added and sonicated for 1 hour. It is left to stand for 24 hours (maceration method). The resulting liquid extract was filtered using filter paper in a Buchner funnel to obtain a maceration filtrate. The filtrate was partitioned using n-hexane and methanol as solvents to separate the polar compounds from the non-polar compounds in leaf extract. The separation process yielded n-hexane and methanol fractions of the leaf extract. The methanol fraction was evaporated using a rotary evaporator at 50°C to remove the methanol solvent and obtain a viscous extract. This extract was diluted with water. The aqueous portion of the leaf extract was stored as a stock solution and used as a medium for nanoparticles and nanocomposite synthesis in this study (Nguyen et al., 2024).

The following phytochemical tests were carried out to identify several groups of alkaloids, flavonoids, diterpenoids, tannins, polyphenols, and saponins which are active ingredients of the leaf extract.

Identification of Alkaloids:

1 mL of leaf extract was mixed with 5 mL of distilled water, followed by addition of 3 mL of HCl and 3 drops of Wagner's reagent. The formation of a brownish-red color indicates the presence of alkaloids (Dahanayake et al., 2019; Makkar et al., 2007).

Identification of Flavonoids:

1 mL of leaf extract was added into 5 mL of distilled water and 1.5 mL of NaOH solution. It was added to the concentrated HCl solution. The formation of a yellow color indicates the presence of flavonoids, and the color faded with the addition of HCl (Adil et al., 2024; Makkar et al., 2007).

Identification of Steroids and Diterpenoids:

1 mL of leaf extract was added dropwise into 2.5 mL of acetic anhydride, 2.5 mL of chloroform, and concentrated H_2SO_4. The formation of red color indicates the presence of terpenoids while dark green color indicates the presence of steroids (Adil et al., 2024; Makkar et al., 2007).

Identification of Tannins and Polyphenols:

1 mL of leaf extract was mixed with 5 mL of distilled water and 1-2 drops of $FeCl_3$. The formation of dark green color indicates the presence of tannins (Adil et al., 2024; Makkar et al., 2007).

Identification of Saponins:

1 mL of leaf extract was placed in a reaction tube. Five milliliters of distilled water was added and shaken vigorously for 30 seconds. The formation of bubbles indicated the presence of saponins in the leaf extract (Adil et al., 2024; Makkar et al., 2007).

2.3.2 Green Synthesis of Nanoparticles and Nanocomposites

Fifty milliliters of 0.1 M zinc nitrate solution [$Zn(NO_3)_2$] was supplemented with *Syzygium polyanthum* (Wight) Walp. leaf extract was constantly stirred using a magnetic stirrer at 90 °C until a paste was formed. The paste was calcined at 550 °C for 4 h to obtain ZnO nanoparticles. The ZnO nanoparticles were characterized using a UV-Vis DRS, FTI-R, XRD, PSA, SEM-EDX, and TEM (Bandeira et al., 2020). Same procedure was conducted for the synthesis of Fe_2O_3 nanoparticles from $Fe(NO_3)_3$ solution and ZnO-Fe_2O_3 nanocomposite from the solution of $Zn(NO_3)_2$, 0.1 $Fe(NO_3)_3$ (Pallela et al., 2019; Sebehanie, 2017). area (Anuar et al., 2021).

Table 1. Phytochemical Test Results for *Syzygium polyanthum* (Wight) Walp. Leaf Extract

Secondary Metabolites	Crude Extract	Hexane Fraction	Methanol Fraction	Water Fraction
Alkaloids	-	-	+	+
Flavonoids	-	+	-	-
Steroids	-	+	-	-
Diterpenoids	-	-	+	+
Tannin and Polyphenols	-	-	+	+
Saponin	+	-	+	-

2.4 Identification of ZnO-Fe_2O_3 Nanocomposite

2.4.1 Preparation of Al/Mg/KNO_3 Pyrotechnic Powder Without and With ZnO-Fe_2O_3 Nanocomposite

KNO_3 was ground in a planetary ball mill and sieved through a 170-mesh vibrating sieve. Al, Mg, and KNO_3 were weighed in weight ratios according to the composition, mixed and stirred in a special pyrotechnic ball mill to obtain a homogeneous mixture. ZnO-Fe_2O_3 nanocomposite was added into the mixture in weight ratios according to the composition. The same method was performed to obtain a homogeneous mixture (Sivapirakasam et al., 2010).

3. RESULTS AND DISCUSSION

3.1 Phytochemical Test

Phytochemical activity tests were conducted to reveal the active compounds which are secondary metabolites contained in the

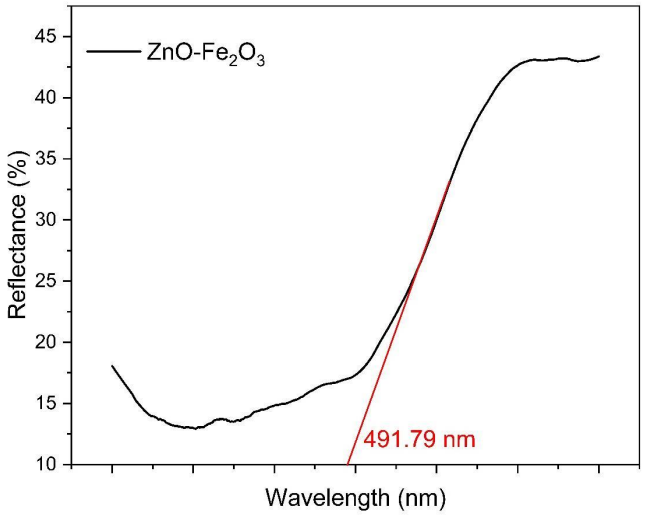

Figure 1. Results of UV-Vis DRS Characterization of $ZnO\text{-}Fe_2O_3$ Nanocomposite

leaf extract. The results are listed in Table 1. Alkaloids, diterpenoids, tannin, and polyphenols contents in aqueous extract are in agreement with previous results (Widjajakusuma et al., 2019). The absence of flavonoids, steroids, and saponin can be caused by the location on where *Syzygium polyanthum* (Wight) Walp. live (Bohm, 2009). The plants that live in the coast have specific secondary metabolites which are distinguishable from plants live in other

The characterization of $ZnO\text{-}Fe_2O_3$ nanocomposite using a UV-Vis DRS aims to identify the $ZnO\text{-}Fe_2O_3$ nanocomposites based on the maximum absorption. The result is presented in Figure 1. There, notably, an absorption at the wavelength of 491.79 nm is identified. Based on previous study conducted by Kebede Gamo Sebehanie, 2017, the absorption is the characteristic of $ZnO\text{-}Fe_2O_3$ nanocomposite (Sebehanie, 2017). To be noticed, the absence of other absorption peaks in the spectrum confirms that the synthesized product is a pure $ZnO\text{-}Fe_2O_3$ nanocomposite.

The Kubelka-Munk function are used to calculate the bandgap energy from the DRS data by plotting the hv of the abscissa and the $(F(R)h\nu)n$ data on the ordinate, where $F(R)$ is the Kubelka-Munk function shown in Equations 1 - 6 (Amoli et al., 2023; Sharma et al., 2019).

$$F(R) = \frac{K}{S} \quad (1)$$

$$K = (1 - R)^2 \quad (2)$$

$$S = 2R \quad (3)$$

$$R = \frac{\%R}{100} \quad (4)$$

Where K is the molar absorption coefficient, S is the scattering coefficient, and R is the reflectance of the material (Sharma et al., 2019). In $(F(R)h\nu)n$, $n = \frac{1}{2}$ for the indirect type and $n = 2$ for the direct type (Sharma et al., 2019).

$$h\nu\nu = \frac{1240}{\lambda} \quad (5)$$

$$\text{Optical band gap} = (F(R)h\nu)^n \quad (6)$$

The band gap energy is calculated based on the numerical derivation of the optical absorption coefficient (α), photon energy ($h\nu$), using the Tauc relationship between the constant (A), and the direct band gap energy (Eg) in Figure 2. The band gap energy value of $ZnO\text{-}Fe_2O_3$ nanocomposite is 1.93 eV, which is consistent with the previously reported values (Amoli et al., 2023).

The success of green synthesis of ZnO and Fe_2O_3 nanoparticles as well as $ZnO\text{-}Fe_2O_3$ nanocomposites are conducted by using FT-IR spectroscopy. It identifies the functional groups in them and the leaves extract (Stuart, 2004). The results are presented in Figure 3. There, on the spectrum of leaves extract, the prominent peaks are 3323, 2135, 1647, 1016, and 690 cm^{-1}. A wide peak at 3323 cm^{-1} indicates overlapped peaks of hydroxyl group from polyphenol and N−H stretching from alkaloids (Makkar et al., 2007; Stuart, 2004). The hydroxyl group can also be from tannin (Makkar et al., 2007; Stuart, 2004). A peak at 1647 cm^{-1} is assigned as C=C stretching from diterpene (Makkar et al., 2007; Stuart, 2004). All of those chemicals are in agreement with results in Table 1. In green synthesis, polar part of secondary metabolites reacts coordinatively with metal atom of nanoparticles (Gulati et al., 2018; Javed et al., 2020). On the other side, non-polar hydrocarbon part of secondary metabolites acts as a tail which interacts with surrounding medium (Gulati et al., 2018; Javed et al., 2020). With this mechanism, secondary metabolites prevent the formation of a large particle or composite (Gulati et al., 2018).

Figure 3 shows the bond between Fe(III)−O observed at wavenumber 570.95 cm^{-1} and Zn−O stretching at 457.15 cm^{-1} (Abbas et al., 2020). A shift in wavenumbers is obvious in the $ZnO\text{-}Fe_2O_3$ nanocomposite compared to the individual ZnO and Fe_2O_3 nanoparticles. A new absorption peak emerges at 1122.62 cm^{-1}, which can indicate formation of a new bond between ZnO and Fe_2O_3.

The determination of the crystal size and crystallinity of the $ZnO\text{-}Fe_2O_3$ nanocomposites was analysed based on diffraction peaks on XRD results. Calcination at a temperature of 550°C for 4 hours produces a $ZnO\text{-}Fe_2O_3$ nanocomposite which has a 2θ value of 34.93°; 37.04°; 41.34°; 50.17°; 55.82°; 62.62°; 66.85°; 73.82°; 81.25°; 88.14°. A slight shift in 2θ value can be seen when compared to the XRD diffraction patterns of the individual nanoparticles, especially ZnO and Fe_2O_3 (Figure 4). The 2θ values of $ZnO\text{-}Fe_2O_3$ nanocomposites are similar to those of $ZnFe_2O_4$ nanocomposites obtained in previous studies by referring to the JCPDS reference card no: 01-089-1397: 31.737°; 34.379°; 36.215°; 47.484°; 56.536°; 62.777°; 66.304°; 67.868°; 69.009°; 72.465°; 76.867°; 81.270°; 89.492° (Abbas et al., 2020). Furthermore, 2θ value of

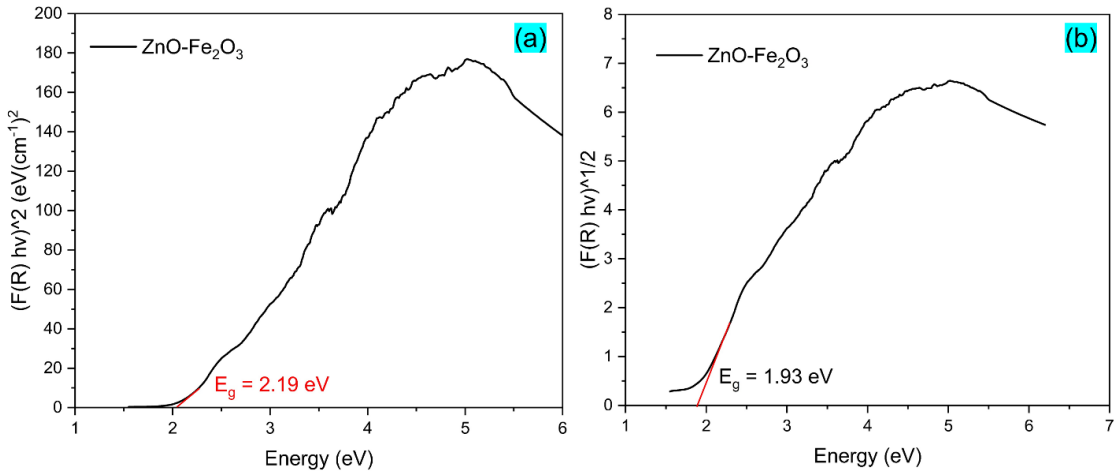

Figure 2. Band Gap Energy of $ZnO\text{-}Fe_2O_3$ Nanocomposite, (a) Direct; (b) Indirect

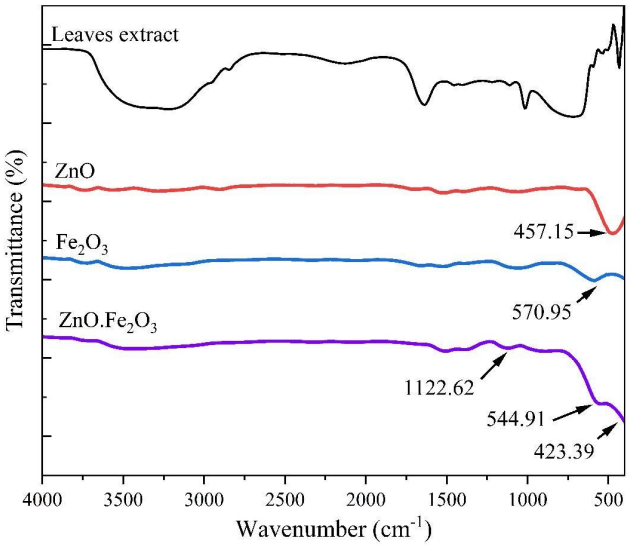

Figure 3. FT-IR Spectroscopy Characterization of: Leaves extract, ZnO, and Fe_2O_3 Nanoparticles, $ZnO\text{-}Fe_2O_3$ Nanocomposite

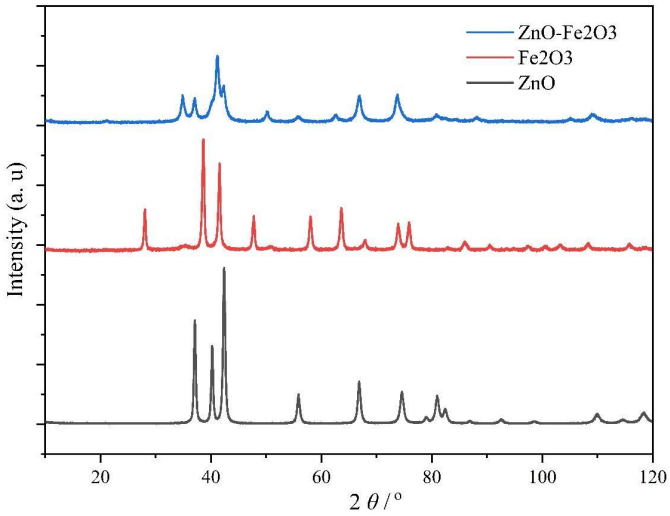

Figure 4. XRD Characterization Results of $ZnO\text{-}Fe_2O_3$ Nanocomposite, Fe_2O_3 and ZnO Nanoparticles

$ZnO\text{-}Fe_2O_3$ nanocomposite can indicate the phase of the crystal of which 34.93° is a sign for trigonal phase, while 50.17° is diffraction from tetragonal phase, 66.85° is for cubic phase (Abdullah et al., 2024). However, since the XRD of $ZnO\text{-}Fe_2O_3$ nanocomposite still presents a value of 2θ ZnO at 41.34°, it can be deduced that the obtained results are $ZnO\text{-}Fe_2O_3$ nanocomposite and ZnO nanoparticles (Abbas et al., 2020). To calculate the crystal size and average crystal size from the XRD data, the Scherrer Equation (Equations 7 and 8) is used (Lifshin, 1999).

$$D = \frac{k\lambda}{\beta \cos\theta} \tag{7}$$

where D is the crystal size (nm), k = 0.94 is the Scherrer constant, λ = 0.154 nm is the wavelength of the X-rays, β is the Full Width at Half Maximum (FWHM) of each characteristic peak (in radians), and θ is the diffraction angle (in radians) (Lifshin, 1999)

$$D = \frac{0.9 \times 0.15406}{\text{radians}(\beta) \times \cos(\text{radians}(\frac{2\theta}{2}))} \tag{8}$$

The calculation of the crystal size of the $ZnO\text{-}Fe_2O_3$ nanocomposite using the Scherrer equation is presented in Table 2. The crystal size of the $ZnO\text{-}Fe_2O_3$ nanocomposite is 7.45 nm.

Characterization using PSA aims to determine the particle size distribution of $ZnO\text{-}Fe_2O_3$ nanocomposite. As shown in Figure 5, the average size is defined as 309.1 nm with polydispersity of 0.248. The results of particle size measurements using PSA measurements are usually larger than those of TEM

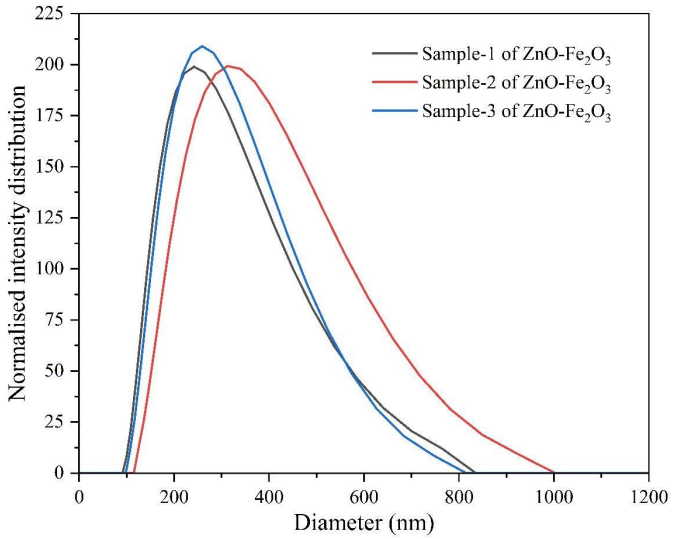

Figure 5. PSA Characterization of ZnO-Fe_2O_3 Nanocomposite

Table 2. Calculation of ZnO-Fe_2O_3 Nanocomposite Crystal Size Using the Scherrer Equation

Peak Position (2θ(°))	β(°)	Crystallite Size Diameter (nm)
34.933	0.974	8.547
37.037	1.140	7.349
41.344	2.245	3.782
50.172	0.869	10.091
55.823	1.051	8.550
62.620	1.023	9.092
66.853	1.142	8.336
73.822	1.368	7.261
81.254	3.382	3.095
88.137	1.316	8.400
	Average D (nm)	7.450

and XRD measurements (Abbas et al., 2020). This contrasting result arises from the different measurement principles of the three instruments (Lifshin, 1999).

The surface morphology and atomic composition of ZnO-Fe_2O_3 nanocomposite is determined based on the characterization using SEM-EDS (Figure 6). Furthermore, the respective atomic compositions of Zn, Fe, and O based on EDS measurement was 17.77; 22.48; and 59.76%, which indicates that the ratio of values of Zn : Fe : O from the measurement results is 1 : 1 : 3 (Amoli et al., 2023).

The result of SEM image processing is shown in Table 3. The average particle size of ZnO-Fe_2O_3 nanocomposite is 23.628 microns. Based on the circularity (0.599) and roundness (0.631) values, ZnO-Fe_2O_3 nanocomposite is classified as well flower-shaped.

TEM characterization was carried out to determine the inner structure of the ZnO-Fe_2O_3 nanocomposite. The results of TEM characterization are presented in Figure 7. It reveals that a predominantly irregular morphology with a small fraction of the ZnO-Fe_2O_3 nanocomposite being cubic as also supported by XRD data (Abdullah et al., 2024). The more amorphous shape compared to individual nanoparticles allows the formation of nanocomposites with less perfect crystalline structures (Amoli et al., 2023). On the other side, based on the TEM characterization results, the particle size of the nanocomposite can be estimated as 17.37 nm.

3.2 Thermogravimetry / Differential Thermal Analysis (TG-DTA) of Pyrotechnic

Results of DTA and TGA of Al/Mg/KNO_3 pyrotechnic powder without and with the addition of ZnO-Fe_2O_3 nanocomposite are depicted in Figure 8 and Figure 9, respectively. Those curves represent effect of heating on KNO_3 which occurs in 2 phases. The first phase includes transformation (around 130°C), and endothermic (Rugunanan and Brown, 1991). The second phase refers to exothermic decomposition of KNO_3 liquid at above 500°C, 200°C higher than the melting point (Rugunanan and Brown, 1991). The second phase is divided into 2 stages, expressed in the following chemical reactions (Pouretedal and Ebadpour, 2014). The first reaction, decomposition of KNO_3 takes place at around 500°C, while the second reaction, decomposition of KNO_2 takes place at around 600°C (Rugunanan and Brown, 1991).

$$2KNO_3 \rightarrow 2KNO_2 + O_2$$
$$4KNO_2 \rightarrow K_2O + 4NO + O_2$$

Notably, in Figure 8, the addition of ZnO-Fe_2O_3 nanocomposite into the composition of Al/Mg/KNO_3 pyrotechnic powder lower the temperature in the first phase. The transformation of KNO_3 in the material occurs at temperature which is 2.12°C lower than that without ZnO-Fe_2O_3 nanocomposite. The melting point of KNO_3 in the material is also lower as much as 6.42°C than that without ZnO-Fe_2O_3 nanocomposite. It is suggested that ZnO-Fe_2O_3 nanocomposite causes a better heat transferring to KNO_3.

For the second phase in Figure 8, it is noted that the addition of ZnO-Fe_2O_3 nanocomposite successfully reduces the number of decomposition peaks of KNO_3 in Al/Mg/KNO_3 pyrotechnic powder, from 2 peaks to 1 peak. It indicates the catalytic activity of ZnO-Fe_2O_3 nanocomposite. It is suggested that the catalytic mechanism of ZnO-Fe_2O_3 nanocomposite involves not generating intermediate compound in the decomposition process. However, the peak, decomposition temperature (Td), is higher than that without ZnO-Fe_2O_3 nanocomposite. Td of pyrotechnic powder with ZnO-Fe_2O_3 nanocomposite is 534.83°C, while the first Td in exothermic phase of pyrotechnic powder is 518.66°C. The detailed data are listed in Table 4.

Figure 8(a) and (b) shows thermogravimetric curves of Al/Mg/KNO_3 pyrotechnic powder without and with ZnO-Fe_2O_3 nanocomposite. The details of weight loss is listed on

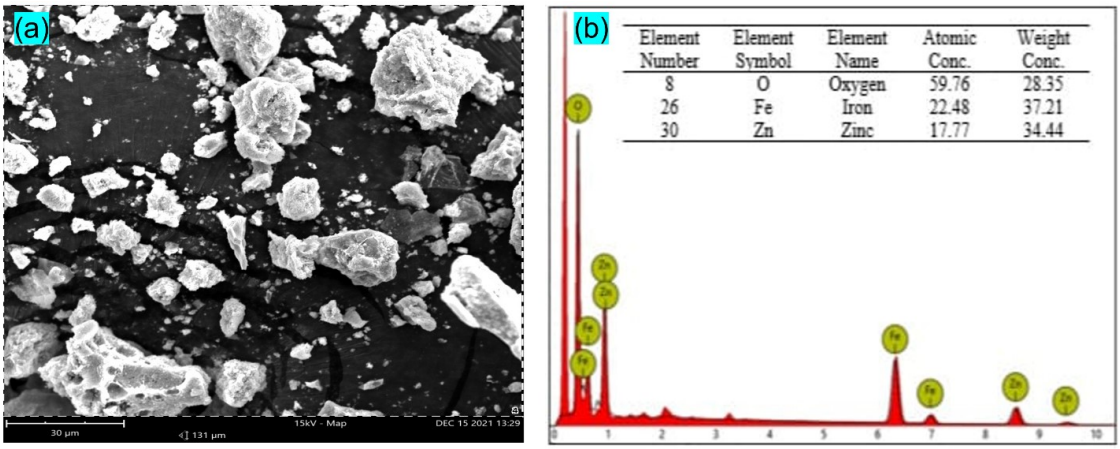

Figure 6. SEM-EDS Identification of ZnO-Fe_2O_3 Nanocomposite, (a) Surface Morphology; (b) Atomic Composition

Table 3. SEM Image Interpretation

Sample	Particle Size (micron)	Circularity	Solidity	Roundness	Aspect Ratio
ZnO-Fe_2O_3	23.628	0.599	0.860	0.631	1.697

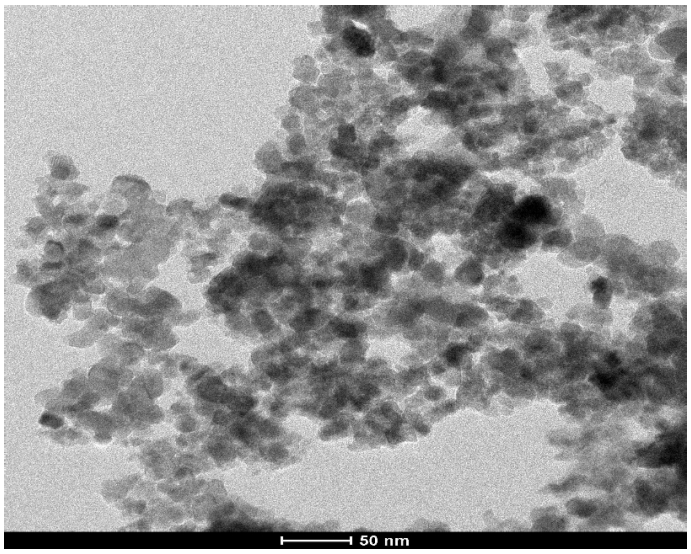

Figure 7. TEM Image of ZnO−Fe_2O_3 Nanocomposite

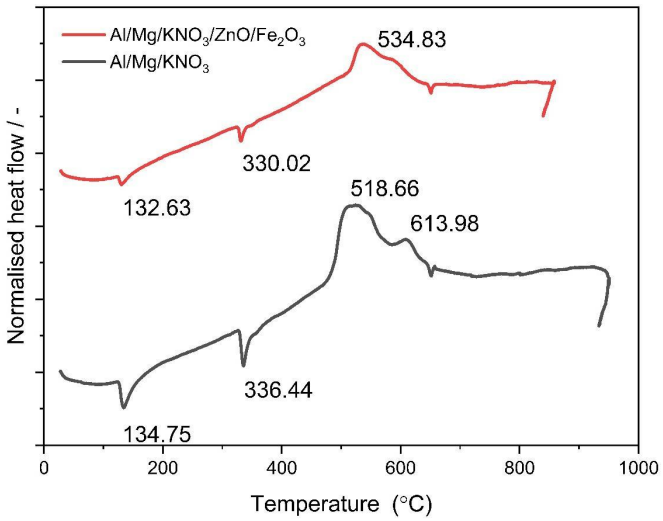

Figure 8. Results of DTA Characterization of Al/Mg/KNO_3 Pyrotechnic Powder without and with the Addition of ZnO-Fe_2O_3 Nanocomposite (Heating Rate 10°C/min)

Table 5. It is noticeable that the pyrotechnic powder with ZnO-Fe_2O_3 nanocomposite has a distinguished weight loss for each stage compared to that without the nanocomposite. In the transformation of KNO_3, ZnO-Fe_2O_3 nanocomposite reduces the weight loss almost 50% of Al/Mg/KNO_3 pyrotechnic powder. In the melting process, weight loss is also reduced by 7.38%. The weight loss in decomposition process is also lower for Al/Mg/KNO_3 pyrotechnic powder with ZnO-Fe_2O_3 nanocomposite. However, as detailed in Table 5, Al/Mg/-KNO_3 pyrotechnic powder with ZnO-Fe_2O_3 nanocomposite has more residual weight than that without ZnO-Fe_2O_3 nanocomposite.

The activation energy Ea (kJ/mol) is calculated using the Kissinger method shown in Equation 9 (Selvakumar et al., 2013):

$$ln\left(\frac{q}{T_{max}^2}\right) = -\frac{Ea}{RT_{max}} \quad (9)$$

where q is the heating rate (K/min), Tmax is the peak temperature (K) and R is the gas constant (8.314 J/(mol.K)). Based on

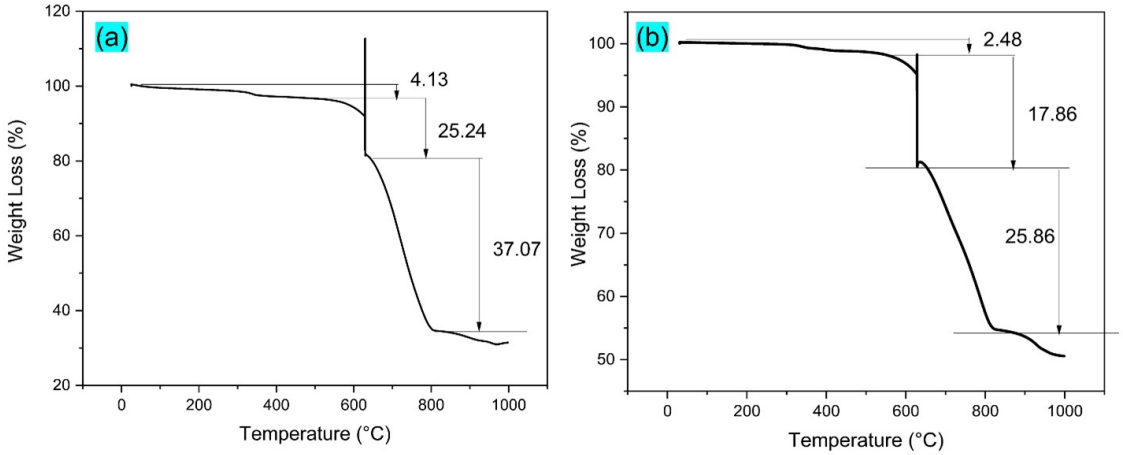

Figure 9. Al/Mg/KNO_3 Pyrotechnic Powder TGA Curve, (a) Without Addition of ZnO- Fe_2O_3 Nanocomposite, (b) with Addition of ZnO-Fe_2O_3 Nanocomposite (Heating Rate 10°C/min)

Table 4. DTA Pyrotechnic Powder Profile

Sample	Weight (mg)	Phase I (Endothermic peak) (°C)		Phase II (Endothermic peak) (°C)	
		Peak 1	Peak 2	Peak 1	Peak 2
Al/Mg/KNO_3	7.714	134.75	336.44	518.66	616.98
Al/Mg/KNO_3/ZnOFe_2O_3	13.482	132.63	330.02	534.83	

Table 5. TGA Pyrotechnic Powder Profile

Sample	Zona	Initial Temperature (°C)	Final Temperature (°C)	Weight Loss (%)	Residue (%)
Al/Mg/KNO_3	1	30	500	4.13	33.56
	2	500	800	62.31	
Al/Mg/KNO_3/ZnOFe_2O_3	1	30	500	2.48	53.8
	2	500	800	43.72	

Figure 8 and Figure 9, peak temperature (temperature at which significant mass loss occurs) of Al/Mg/KNO_3 pyrotechnic powder with ZnO-Fe_2O_3 nanocomposite is 535.57 °C, 81.17 °C lower than pyrotechnic powder without ZnO-Fe_2O_3 nanocomposite. On the other side, activation energy of Al/Mg/KNO_3 pyrotechnic powder with ZnO-Fe_2O_3 nanocomposite is 52.07 kJ/mol, 6.64 kJ/mol lower than pyrotechnic powder without ZnO-Fe_2O_3 nanocomposite. This result is in consistent with the previous result (Azhagurajan et al., 2011).

4. CONCLUSION

ZnO-Fe_2O_3 nanocomposite was successfully synthesized using *Syzygium polyanthum* Wight Walp. leaf extract. According to PSA characterization results, the particle size was 309.1 nm and based on TEM characterization results, the obtained particle size was 17.37 nm. The addition of ZnO-Fe_2O_3 nanocomposite to Al/Mg/KNO_3 pyrotechnic powder reduces the stage of decomposition of the pyrotechnic powder, from two stages to one stage. In the pyrotechnic decomposition process, Al/Mg/KNO_3 pyrotechnic powder generates an intermediate product before the completed decomposition. However, in Al/Mg/KNO_3/ZnO-Fe_2O_3 pyrotechnic powder, no intermediate product is generated because the presence of ZnO-Fe_2O_3 nanocomposite accelerates the decomposition process. ZnO-Fe_2O_3 nanocomposite can reduce the activation energy of KNO_3 decomposition from 58 kJ/mol to 52 kJ/mol.

5. ACKNOWLEDGEMENT

The authors would like to convey our gratitude to the colleagues, researchers, engineers and technicians at the Rocket Technology Research Center, Aeronautics and Space Research Organization, National Research and Innovation Agency and Department of Chemistry, Mathematics and Natural Sciences Faculty, University of Indonesia, for their support.

REFERENCES

Abbas, H. S., A. Krishnan, and M. Kotakonda (2020). Fabrication of Iron Oxide/Zinc Oxide Nanocomposite Using Creeper Blepharis maderaspatensis Extract and Their Antimicrobial Activity. *Frontiers in Bioengineering and Biotechnology*, **8**; 595161

Abdelbaky, A. S., A. M. H. A. Mohamed, M. Sharaky, N. A. Mohamed, and Y. M. Diab (2023). Green Approach for the Synthesis of ZnO Nanoparticles Using *Cymbopogon citratus* Aqueous Leaf Extract: Characterization and Evaluation of Their Biological Activities. *Chemical and Biological Technologies in Agriculture*, **10**(1); 63

Abdelmigid, H. M., N. A. Hussien, A. A. Alyamani, M. M. Morsi, N. M. Alsufyani, and H. A. Kadi (2022). Green Synthesis of Zinc Oxide Nanoparticles Using Pomegranate Fruit Peel and Solid Coffee Grounds vs. Chemical Method of Synthesis, with Their Biocompatibility and Antibacterial Properties Investigation. *Molecules*, **27**(4); 1236

Abdullah, J. A. A., H. Ali Mohammed, C. Salmi, Z. Alqarni, S. Eddine Laouini, A. Guerrero, and A. Romero (2024). Sustainable Synthesis of ZnO and Fe_xO_y Nanoparticles and Their $ZnFe_2O_4$: Comprehensive Characterization and Applications in Antioxidant Activity and Antibiotics Degradation Efficiency. *Bioorganic Chemistry*, **153**; 107828

Adil, M., F. Z. Filimban, A. Ambrin, Quddoos, A. A. Sher, and M. Naseer (2024). Phytochemical Screening, HPLC Analysis, Antimicrobial and Antioxidant Effect of *Euphorbia parviflora* L. (*Euphorbiaceae* Juss.). *Scientific Reports*, **14**(1); 5627

Aegerter, M. A., N. Leventis, M. Koebel, and S. A. Steiner (2023). *Springer Handbook of Aerogels*. Springer

Al-Darwesh, M. Y., S. S. Ibrahim, and M. A. Mohammed (2024). A Review on Plant Extract Mediated Green Synthesis of Zinc Oxide Nanoparticles and Their Biomedical Applications. *Results in Chemistry*, **7**; 101368

Al-Rajhi, A. M. H., T. M. Abdelghany, M. S. Almuhayawi, M. H. Alruhaili, S. K. A. Jaouni, and S. Selim (2024). The Green Approach of Chitosan/Fe_2O_3/ZnO-Nanocomposite Synthesis With an Evaluation of Its Biological Activities. *Applied Biological Chemistry*, **67**(1); 75

Ali, S. K., S. Radu, M. A. R. Nor-Khaizura, and Y. Rukayadi (2022). Antimicrobial Activity of Jambu Mawar [*Syzygium jambos* (L.) Alston] Leaf Extract Against Foodborne Pathogens and Spoilage Microorganisms. *International Food Research Journal*, **29**(6); 1348–1359

Amoli, A. E., M. Masoumi, M. S. Baei, F. Babaei, and G. F. Pasha (2023). Visible Light Mediated Photocatalytic Anionic and Cationic Dyes Degradation Using ZnO-Fe_2O_3 Nanocomposite. *Journal of Water and Environmental Nanotechnology*, **8**(1); 52–65

Anuar, T. A. F. T., A. Ismail, I. F. M. Suffian, A. A. A. Hamid, M. H. Arzmi, and M. N. Omar (2021). LCMS Dataset on Compounds in *Syzygium polyanthum* (Wight) Walp. Leaves Variant From the East Coast of Peninsular Malaysia. *Data in Brief*, **39**; 107485

Azhagurajan, A., N. Selvakumar, and T. L. Thanulingam (2011). Thermal and Sensitivity Analysis of Nano Aluminium Powder for Firework Application. *Journal of Thermal Analysis and Calorimetry*, **105**(1); 259–267

Bandeira, M., M. Giovanela, M. Roesch-Ely, D. M. Devine, and J. d. S. Crespo (2020). Green Synthesis of Zinc Oxide Nanoparticles: A Review of the Synthesis Methodology and Mechanism of Formation. *Sustainable Chemistry and Pharmacy*, **15**; 100223

Bohm, B. A. (2009). *The Geography of Phytochemical Races*. Springer Science and Business Media BV

Buarki, F., H. AbuHassan, F. Al Hannan, and F. Z. Henari (2022). Green Synthesis of Iron Oxide Nanoparticles Using *Hibiscus rosa* Sinensis Flowers and Their Antibacterial Activity. *Journal of Nanotechnology*, **2022**; 1–6

Dahanayake, J. M., P. K. Perera, P. Galappatty, H. D. S. M. Perera, and L. D. A. M. Arawwawala (2019). Comparative Phytochemical Analysis and Antioxidant Activities of *Tamalakyadi decoction* with Its Modified Dosage Forms. *Evidence-Based Complementary and Alternative Medicine*, **2019**(1); 6037137

Dave, P. N., P. N. Ram, and S. Chaturvedi (2016). Transition Metal Oxide Nanoparticles: Potential Nano-Modifier for Rocket Propellants. *Particulate Science and Technology*, **34**(6); 676–680

Faisal, S., H. Jan, S. A. Shah, S. Shah, A. Khan, M. T. Akbar, M. Rizwan, F. Jan, Wajidullah, N. Akhtar, A. Khattak, and S. Syed (2021). Green Synthesis of Zinc Oxide (ZnO) Nanoparticles Using Aqueous Fruit Extracts of *Myristica fragrans*: Their Characterizations and Biological and Environmental Applications. *ACS Omega*, **6**(14); 9709–9722

Goncalves, R., J. A. F. F. Rocco, and K. Iha (2017). *Energetic Materials Research, Applications, and New Technologies*. International Publisher of Information Science and Technology Research

Gulati, S., M. Sachdeva, and K. K. Bhasin (2018). Capping Agents in Nanoparticle Synthesis: Surfactant and Solvent System. *AIP Conference Proceedings*, **1953**(1); 030214

Hatakeyama, T., Z. Liu, and J. Wiley (1998). *Handbook of Thermal Analysis*. John Wiley & Sons

Ineichen, H. and B. Berger (2004). Pyrotechnics in Fireworks. *Chimia*, **58**(6); 369–373

Islam, M. F., S. Islam, M. A. S. Miah, A. K. O. Huq, A. K. Saha, Z. J. Mou, M. M. H. Mondol, and M. N. I. Bhuiyan (2024). Green Synthesis of Zinc Oxide Nanoparticles Using *Allium cepa* L. Waste Peel Extracts and Its Antioxidant and Antibacterial Activities. *Heliyon*, **10**(3); e25430

Javed, R., M. Zia, S. Naz, S. O. Aisida, N. ul Ain, and Q. Ao (2020). Role of Capping Agents in the Application of Nanoparticles in Biomedicine and Environmental Remediation: Recent Trends and Future Prospects. *Journal of Nanobiotechnology*, **18**(172); 1–15

Khan, S., Y. Rukayadi, A. H. Jaafar, and N. H. Ahmad (2023). Antibacterial Potential of Silver Nanoparticles

(SP-AgNPs) Synthesized from *Syzygium polyanthum* (Wight) Walp. Against Selected Foodborne Pathogens. *Heliyon*, **9**; e22771

Kharissova, O. V., B. I. Kharisov, C. M. O. González, Y. P. Méndez, and I. López (2019). Greener Synthesis of Chemical Compounds and Materials. *Royal Society Open Science*, **6**(191378); 191378.

Kiwumulo, H. F., H. Muwonge, C. Ibingira, M. Lubwama, J. B. Kirabira, and R. T. Ssekitoleko (2022). Green Synthesis and Characterization of Iron-Oxide Nanoparticles Using *Moringa oleifera*: A Potential Protocol for Use in Low and Middle Income Countries. *BMC Research Notes*, **15**(1); 149

Lackner, M., A. B. Palotás, and F. Winter (2013). *Combustion from Basics to Applications*. John Wiley & Sons, first edition

Lakshmnarayanan, S., M. F. Shereen, K. L. Niraimathi, P. Brindha, and A. Arumugam (2021). One-Pot Green Synthesis of Iron Oxide Nanoparticles from *Bauhinia tomentosa*: Characterization and Application Towards Synthesis of 1,3 Diolein. *Scientific Reports*, **11**(1); 8643

León, D., I. Amez, M. Radojevic, N. Manic, D. Stojiljkovic, A. Milivojevic, J. García-Torrent, and B. Castells (2024). Emissions and Fire Risk Assessment of Nitrocellulose As a Sustainable Alternative in Pyrotechnic Compositions. *Fire*, **7**(8); 265

Lestariana, E., Y. Yulizar, and H. Supriyatno (2024). Green Synthesis and Characterization of Zinc Oxide (ZnO) Nanoparticles Using *Syzygium polyanthum* (wight) Walp. Aqueous Leaf Extract and Their Application in Al/Mg/-KNO_3 Pyrotechnics. *AIP Conference Proceedings*, **3074**(1); 070009

Lifshin, E. (1999). *X-Ray Characterization of Materials*. Wiley-VCH

Makkar, H. P. S., P. Siddhuraju, and K. Becker (2007). *Plant Secondary Metabolites*. Humana Press

Mohamed, A., R. R. Atta, A. A. Kotp, F. I. Abo El-Ela, H. Abd El-Raheem, A. Farghali, D. H. M. Alkhalifah, W. N. Hozzein, and R. Mahmoud (2023). Green Synthesis and Characterization of Iron Oxide Nanoparticles for the Removal of Heavy Metals (Cd^{2+} and Ni^{2+}) from Aqueous Solutions with Antimicrobial Investigation. *Scientific Reports*, **13**(1); 7227

Naiel, B., M. Fawzy, M. W. A. Halmy, and A. E. D. Mahmoud (2022). Green Synthesis of Zinc Oxide Nanoparticles Using Sea Lavender (*Limonium pruinosum* L. Chaz.) Extract: Characterization, Evaluation of Anti-Skin Cancer, Antimicrobial and Antioxidant Potentials. *Scientific Reports*, **12**(1); 20370

Nguyen, K. D. H., T. D. Manh, B. X. Vuong, L. T. P. Nguyen, D. T. Vu, T. L. Huynh, and K. L. D. Ngo (2024). *Syzygium polyanthum* (Wight) Walp. Leaf Extract as a Sustainable Corrosion Inhibitor for Carbon Steel in Hydrochloric Acidic Environment. *Journal of Industrial and Engineering Chemistry*, **143**; 468–487

Osman, A. I., Y. Zhang, M. Farghali, A. K. Rashwan, A. S. Eltaweil, E. M. Abd El-Monaem, I. M. A. Mohamed, M. M. Badr, I. Ihara, D. W. Rooney, and P. S. Yap (2024). Synthesis of Green Nanoparticles for Energy, Biomedical, Environmental, Agricultural, and Food Applications: A Review. *Environmental Chemistry Letters*, **22**(2); 841–887

Pallela, P. N. V. K., S. Ummey, L. K. Ruddaraju, S. Gadi, C. S. L. Cherukuri, S. Barla, and S. V. N. Pammi (2019). Antibacterial Efficacy of Green Synthesized α-Fe_2O_3 Nanoparticles Using Sida Cordifolia Plant Extract. *Heliyon*, **5**(11); e02765

Pouretedal, H. R. and R. Ebadpour (2014). Application of Non-Isothermal Thermogravimetric Method to Interpret the Decomposition Kinetics of $NaNO_3$, KNO_3, and $KClO_4$. *International Journal of Thermophysics*, **5**; 942–951

Ravanbod, M. and H. R. Pouretedal (2016). Catalytic Effect of Fe_2O_3, Mn_2O_3, and TiO_2 Nanoparticles on Thermal Decomposition of Potassium Nitrate. *Journal of Thermal Analysis and Calorimetry*, **124**; 1091–1098

Restasari, A., R. Ardianingsih, L. H. Abdillah, and K. Hartaya (2024). Preliminary Research of Natural Oils as Green Flow Properties Modifiers of Hydroxyl Terminated Polybutadiene (HTPB). **2860**(1); 030005

Reyes-Perez, J. A., G. Roa-Morales, C. A. De Leon-Condes, and P. Balderas-Hernandez (2023). Nanocomposites from Spent Coffee Grounds and Iron/Zinc Oxide: Green Synthesis, Characterization, and Application in Textile Wastewater Treatment. *Water Science and Technology*, **88**(6); 1547–1563

Rugunanan, R. A. and M. E. Brown (1991). Reactions of Powdered Silicon with Some Pyrotechnic Oxidants. *Journal of Thermal Analysis*, **37**(6); 1193–1211

Sebehanie, K. G. (2017). Comparative Study of ZnO/Fe_2O_3 Nanocomposite Sensitized with Natural Pigments for Dye Sensitized Solar Cell. *International Journal of Hybrid Information Technology*, **10**(1); 199–214

Selvakumar, N., A. Azhagurajan, and A. Suresh (2013). Experimental Analysis on Nano Scale Flash Powder Composition in Fireworks Manufacturing. *Journal of Thermal Analysis and Calorimetry*, **113**(2); 615–621

Sharma, M., A. Yangui, V. R. Whiteside, I. R. Sellers, D. Han, S. Chen, M. H. Du, and B. Saparov (2019). $Rb_4Ag_2BiBr_9$: A Lead-Free Visible Light Absorbing Halide Semiconductor with Improved Stability. *Inorganic Chemistry*, **58**(7); 4446–4455

Sivapirakasam, S. P., M. Surianarayanan, and F. Chandrasekaran (2010). Thermal Characterization of Pyrotechnic Flash Compositions. *Science and Technology Energetic Materials*, **71**(1); 11–16

Stuart, B. H. (2004). *Infrared Spectroscopy: Fundamentals and Application*. John Wiley & Sons Ltd

Thi, T. U. D., T. T. Nguyen, Y. D. Thi, K. H. Ta Thi, B. T. Phan, and K. N. Pham (2020). Green Synthesis of ZnO Nanoparticles Using Orange Fruit Peel Extract for Antibacterial Activities. *RSC Advances*, **10**(40); 23899–23907

Widjajakusuma, E. C., A. Jonosewojo, L. Hendriati, S. Wijaya, Ferawati, A. Surjadhana, W. Sastrowardoyo, N. Monita, N. M. Muna, R. P. Fajarwati, M. Ervina, S. Y. Esar, L. Soegianto, T. Lang, and C. Heriyanti (2019). Phytochemical

Screening and Preliminary Clinical Trials of the Aqueous Extract Mixture of *Andrographis paniculata* (Burm. f.) Wall. ex Nees and *Syzygium polyanthum* (Wight.) Walp Leaves in Metformin Treated Patients with Type 2 Diabetes. *Phytomedicine*, **55**; 137–147

Yaou Balarabe, B., M. N. Illiassou Oumarou, A. S. Koroney, I. Adjama, and A. R. Ibrahim Baraze (2023). Photo-Oxidation of Organic Dye by Fe_2O_3 Nanoparticles: Catalyst, Electron Acceptor, and Polyurethane Membrane (PU-Fe_2O_3) Effects. *Journal of Nanotechnology*, **2023**(1); 1292762

Ying, S., Z. Guan, P. C. Ofoegbu, P. Clubb, C. Rico, F. He, and J. Hong (2022). Green Synthesis of Nanoparticles: Current Developments and Limitations. *Environmental Technology and Innovation*, **26**; 102336

Zheng, D., J. Wang, Y. Duo, Z. Fang, C. Yu, M. Qiao, and J. Liu (2022). Experimental Insight into Co-Pyrolysis Mechanism of 5-Amino 1H-Tetrazole/Nitrocellulose Based Pyrotechnic. *Journal of Analytical and Applied Pyrolysis*, **167**; 105669

Zunigaga-Miranda, J., J. Guerra, A. Mueller, A. Mayorga-Ramos, S. E. Carrera-Pacheco, C. Barba-Ostria, J. Heredia-Moya, and L. P. Guamán (2023). Iron Oxide Nanoparticles: Green Synthesis and Their Antimicrobial Activity. *Nanomaterials*, **13**(22); 2919

